JACS
JOURNAL OF THE AMERICAN CHEMICAL SOCIETY

Article

pubs.acs.org/JACS

Application of Visible Light Photocatalysis with Particle Lithography To Generate Polynitrophenylene Nanostructures

Susan D. Verberne-Sutton, Rashanique D. Quarels, Xianglin Zhai, Jayne C. Garno, and Justin R. Ragains*

Department of Chemistry, Louisiana State University, 232 Choppin Hall, Baton Rouge, Louisiana 70803, United States

Supporting Information

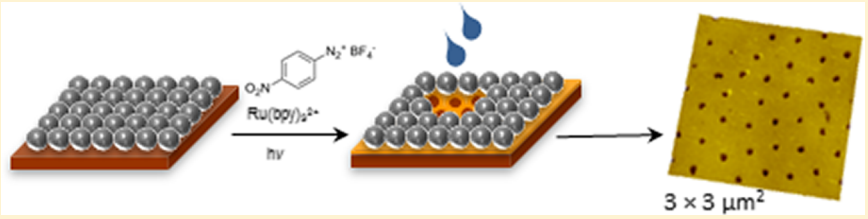

ABSTRACT: Visible light photoredox catalysis was combined with immersion particle lithography to prepare polynitrophenylene organic films on Au(111) surfaces, forming a periodic arrangement of nanopores. Surfaces masked with mesospheres were immersed in solutions of *p*-nitrobenzenediazonium tetrafluoroborate and irradiated with blue LEDs in the presence of the photoredox catalyst $Ru(bpy)_3(PF_6)_2$ to produce *p*-nitrophenyl radicals that graft onto gold substrates. Surface masks of silica mesospheres were used to protect small, discrete regions of the Au(111) surface from grafting. Nanopores were formed where the silica mesospheres touched the surface; the mask effectively protected nanoscopic local areas from the photocatalysis grafting reaction. Further reaction of the grafted arenes with aryl radicals resulted in polymerization to form polynitrophenylene structures with thicknesses that were dependent on both the initial concentration of diazonium salt and the duration of irradiation. Photoredox catalysis with visible light provides mild, user-friendly conditions for the reproducible generation of multilayers with thicknesses ranging from 2 to 100 nm. Images acquired with atomic force microscopy (AFM) disclose the film morphology and periodicity of the polymer nanostructures. The exposed sites of the nanopores provide a baseline to enable local measurements of film thickness with AFM. The resulting films of polynitrophenylene punctuated with nanopores provide a robust foundation for further chemical steps. Spatially selective binding of mercaptoundecanoic acid to exposed sites of Au(111) was demonstrated, producing a periodic arrangement of thiol-based nanopatterns within a matrix of polynitrophenylene.

INTRODUCTION

Covalently bound films produced with electrochemical reduction of diazonium salts are more stable than surface layers produced by chemisorption of *n*-alkanethiols, providing benefits as electrochemical sensor surfaces that require long-term storage or repeated chemical cycling.[1,2] A limitation of electrografting is that the surface must be comprised of conductive or semiconductor materials. Electrochemical reduction of salts has been used to graft organic films to surfaces of gold,[3−6] iron,[7] silicon,[8,9] carbon,[10−18] diamond,[19] platinum,[20] indium−tin−oxide,[21,22] and highly oriented pyrolytic graphite[23,24] electrodes in either organic or aqueous media. Electrochemical reduction of arenediazonium salts was accomplished with Co, Ni, Cu, Zn, Pt, and Au substrates.[25] The surface layers generated by electrochemical reduction are typically less than 10 nm in thickness and attach covalently to the electrode. Organic films formed from reduction of diazonium salts offer flexibility for selecting diverse molecules to design surface properties and reactivity. A broad range of derivatives of diazonium salts have been electrografted, including those of tetraarylporphyrin,[11] anthraquinone,[4,5] bithiophene phenyl,[26] 4-carboxybenzene,[24] 4-nitrobenzene,[3,9,10,16,18−21,27−29] 4-aminobenzene,[6,14] 4-fluorenephenyl,[21] and 4-decylbenzene.[27] With further chemical steps the grafted films can be used to build multilayered surface structures.[30−33]

Photochemical approaches with diazonium salts have not been widely investigated for grafting organic films to surfaces.[34] Visible light photocatalysis can be used with diazonium salts in the presence of a photoredox catalyst to produce carbon-centered radicals that undergo processes that include grafting to both conducting and non-conducting surfaces under mild, user-friendly conditions.[34−38] Visible light photocatalytic grafting of arenediazonium salts was accomplished by Bouriga et al. using the photocatalyst $Ru(bpy)_3(PF_6)_2$ with both Au(111) and the non-conductive polymer surface of polyvinyl chloride.[34] A similar visible light photocatalytic approach for the surface-patterning of coumarin-modified cellulose was reported by Schroll et al.[35] Irradiation with UV light was used to photochemically reduce 4-(2-(4-pyridinyl)ethynyl)benzenediazonium salt to form a film on quartz substrates, as reported by Zhao et al.[31] Ultraviolet irradiation of the charge transfer complex of 1,4-dimethoxybenzene and the nitrobenzene-

Received: June 2, 2014
Published: September 22, 2014

   dx.doi.org/10.1021/ja505521k | J. Am. Chem. Soc. 2014, 136, 14438−14444

diazonium cation resulted in the grafting of metal surfaces (Au, Cu, Fe), reported by Busson et al.[39]

Surface patterning has been accomplished with organic films produced by electrochemical reduction of diazonium salts using methods developed with scanning electrochemical microscopy (SECM),[40] microcontact printing,[41,42] scanning probe-based nanolithography,[9,10,43] electrografting,[44] and particle lithography.[21,33,45,46] The combination of particle lithography with molecular surface assembly is a practical strategy for preparing periodic nanostructures with high throughput.[47]

In the work described herein, visible light photocatalysis was combined with particle lithography to successfully generate films of polynitrophenylene with designed thickness on Au(111). The films of polynitrophenylene were prepared by visible light irradiation of $Ru(bpy)_3(PF_6)_2$ in the presence of 4-nitrobenzenediazonium tetrafluoroborate. Our strategy for nanofabrication applied particle lithography with surface masks consisting of silica mesospheres (d = 500 nm) to protect small, discrete regions of the surface from the photocatalytic grafting reaction. After steps of photografting, the exposed sites of nanopores were backfilled with 11-mercaptoundecanoic acid (MUA) to generate a compositionally patterned surface composed of MUA nanostructures within a matrix film of polynitrophenylene.

EXPERIMENTAL SECTION

Materials and Reagents. Sodium nitrite (99.8% ACS certified) was obtained from Fisher Scientific. $Ru(bpy)_3(PF_6)_2$ (97%), 4-nitroaniline (99%), tetrafluoroboric acid (48% aqueous), anhydrous diethyl ether (99.0% ACS reagent grade), acetone (99.5% ACS reagent grade), and mercaptoundecanoic acid (95%) were purchased from Sigma-Aldrich and used without further purification. ^{1}H NMR and ^{13}C NMR spectroscopy were performed on a Bruker AV-400 spectrometer. Unless otherwise noted, all materials were purchased from Sigma-Aldrich and used without further purification. Glassware was flame-dried under vacuum and backfilled with dry nitrogen prior to use. Deuterated solvents were obtained from Cambridge Isotope Labs. Acetonitrile for grafting procedures was purified according to the method published by Pangborn et al.[48] The irradiation source for photografting reactions was two 4W sapphire blue LED flex strips from Creative Lighting Solutions (Cleveland, OH).

Preparation of Gold Surfaces with a Mesosphere Mask. Two types of substrates were used for preparing samples. Ultraflat gold films were prepared on mica(0001) by evaporative deposition. Template-stripped, gold substrates were prepared by a previously reported procedure.[49] Glass discs were glued to freshly prepared gold films using an epoxy (EPO-TEK, Billerica, MA). Pieces of ultraflat gold/glass were stripped from mica to expose a clean, atomically flat Au(111) surface. Size-sorted silica mesospheres with an average diameter of 500 nm (Thermo Scientific) were cleaned by centrifugation and suspension in water (three cleaning cycles). A 40 μL drop of the silica mesosphere suspension was placed onto the template-stripped gold substrates, dried in air for 2 h, and then oven-dried at 150 °C for at least 14 h. The final heating step was used to temporarily anneal the silica spheres to the substrate to prevent displacement during chemistry steps of immersion in solutions. After completion of the steps of the chemical reactions, removal of the surface mask was accomplished by sonication in clean solvents.

Preparation of 4-Nitrobenzenediazonium Tetrafluoroborate (NBDT). The NBDT was prepared according to a method similar to that reported by Vogel using 4-nitroaniline.[50] Tetrafluoroboric acid (HBF_4, 3.6 mL, 27 mmol) was added to a round-bottom flask containing 5 mL of deionized water. A solution of 4-nitroaniline (1.40 g, 10 mmol) was added in three portions to the round-bottom flask and stirred. The resulting olive-green solution was cooled to 0 °C in an ice−water bath. A solution of sodium nitrite (0.69 g, 10 mmol) in deionized water (2 mL) was prepared and then added dropwise to the aqueous solution of 4-nitroaniline and HBF_4 over a period of 30 min under N_2 at 0 °C. As the resulting cloudy green mixture became difficult to stir, the stirring rate was increased. The round-bottom flask was wrapped in foil, and the mixture was stirred for an additional 1 h at 0 °C. The resulting mixture was filtered and washed with 2 mL of cold deionized water. The resulting solid was added to a 250 mL Erlenmeyer flask and dissolved in 30 mL of acetone. The remaining precipitate was removed by filtration and washed with 2 mL of acetone. Twenty milliliters of anhydrous diethyl ether was added at once to the resulting filtrate. The precipitated diazonium salt was filtered using a Büchner funnel, washed with 10 mL of anhydrous diethyl ether, and dried under high vacuum for 1 h. Due to its low stability at room temperature, the diazonium salt was used immediately or stored at −2 °C prior to use. A total of 1.2344 g (52.1%) of $C_6H_4N_3O_2BF_4$ was isolated. ^{1}H NMR (400 MHz, CD_3CN): δ 8.74 (d, 2H, J = 9.32 Hz), 8.63 (d, 2H, J = 9.32 Hz). ^{13}C NMR (100 MHz, CD_3CN): δ 155.3, 135.5, 126.7, 121.6. The NMR spectra can be found in Supporting Information, Figures S1 and S2.

Photografting Procedure. Acetonitrile (MeCN) from a solvent purification system[48] was dried over 3 Å molecular sieves for 24 h. A solution of NBDT (47.4 mg, 0.2 mmol) and $Ru(bpy)_3(PF_6)_2$ (3.0 mg, 0.005 mmol) in 2 mL of anhydrous MeCN was wrapped in foil, stirred, and deoxygenated three times using the freeze−pump−thaw protocol. A lower concentration (10^{-3} M) of NBDT was prepared via dilution. A 20 μL aliquot of the 10^{-1} M solution of NBDT was transferred to a separate round-bottom flask wrapped in foil. Anhydrous MeCN (1.98 mL) was then added to achieve the desired concentration (10^{-3} M). This solution was also deoxygenated three times using the freeze−pump−thaw protocol. An egg-shaped stir bar and the masked gold substrate were physically separated inside of a 125 mL Erlenmeyer flask so that the stir bar did not touch the masked gold substrate. The Erlenmeyer flask was sealed with a rubber septum and purged with a continuous flow of nitrogen for 30 min (see Supporting Information, Figure S3). The deoxygenated solution of NBDT and $Ru(bpy)_3(PF_6)_2$ in anhydrous MeCN was added to the 125 mL Erlenmeyer flask containing the masked gold sample and stir bar. The suspension was magnetically stirred and irradiated. After irradiation for the desired period of time, the solution was decanted. The masked gold sample was washed twice with 2 mL of deionized water and twice with 2 mL of ethanol to remove material that was not strongly attached to the gold surface. The samples were sonicated in ethanol for 1 min to remove the mesospheres and any remaining non-covalently bound residues.

Backfilling the Nanopores with Mercaptoundecanoic Acid (MUA). A solution of MUA in ethanol was prepared by adding 0.0014 g of MUA into 10 mL ethanol and stirring until it was completely dissolved (0.6 mM). The solution was injected into a liquid cell (Sonimoto Laboratories, West Bloomfield, MI) that supports imaging samples in a liquid environment. Fresh aliquots (1 mL) of the MUA solution were replenished each hour to replace liquid lost by evaporation.

Atomic Force Microscopy (AFM). The samples were imaged using a model 5500 or model 5420 atomic force microscope with Pico View v.1.12 software (Agilent Technologies, Chandler, AZ). Non-conductive imaging probes from Bruker (MSCT, 0.01−0.6 N/m) were used to acquire contact-mode images. Images were processed and analyzed using Gwyddion (v. 2.22), an open-access processing software designed for AFM images, supported by the Czech Metrology Institute.[51]

RESULTS AND DISCUSSION

To accomplish photografting, gold surfaces masked with mesospheres were immersed in solutions of NBDT in MeCN and irradiated for selected time intervals in the presence of the photocatalyst $Ru(bpy)_3(PF_6)_2$ to produce p-nitrophenyl radicals that grafted onto Au(111). As the reaction proceeds, successive attachment of aryl radicals to grafted arenes generated films of polynitrophenylene (Scheme 1). The mask

dx.doi.org/10.1021/ja505521k | J. Am. Chem. Soc. 2014, 136, 14438−14444

Scheme 1. Photografting Reaction Steps

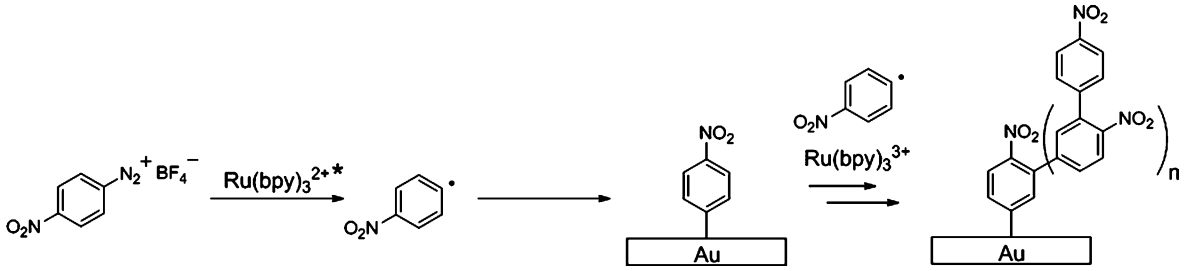

of mesospheres was removed by ultrasonication in ethanol to generate a periodic arrangement of uncovered nanopores in locations where the silica mesospheres covered the substrate. For scanning probe studies, the nanopores provide a useful baseline for measuring the thickness of the films and also provide exposed surfaces sites of the substrate for backfilling with selected molecules.

Photografting of NBDT onto Masked Gold Substrates. A densely packed film of polynitrophenylene was formed after 30 min of irradiation at a concentration of 10^{-3} M NBDT, shown in Figure 1. A periodic arrangement of dark holes is

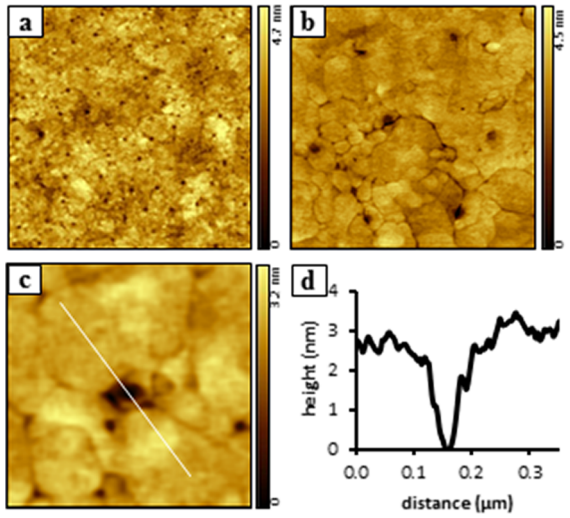

Figure 1. Photografted film of polynitrophenylene formed on Au(111) generated with an initial concentration of 1 mM NBDT, after 30 min of irradiation. Nanopores were produced using immersion particle lithography. (a) Topography image (5 × 5 μm^2) acquired in air; (b) zoom-in view (1.5 × 1.5 μm^2); (c) a single nanopore (500 × 500 nm^2); (d) cursor profile for the line in *c*.

observed throughout areas of the sample. The areas of the nanopores are sites of uncovered substrate where the mesoparticle mask was removed. Approximately 1% of the surface is covered with nanopores in Figure 1A, scaling to a surface density of 10^8 nanopores/cm^2. The sample was prepared with an NBDT concentration of 1 mM and was imaged with contact-mode AFM in ambient air. Features such as terraces, scars, and domain boundaries that are characteristic of the underlying Au(111) substrate are evident within the 5 × 5 μm^2 topography image of Figure 1a. For well-resolved AFM images of thin organic films the features of the underlying Au(111) substrate such as terraces, scars, and domain boundaries can often be detected. For thicker films such features will no longer be resolvable. Interestingly, the films do not exhibit molecular vacancy islands that are characteristic of Au surface reconstruction typically observed with *n*-alkanethiol monolayers.[52] The dense film has 77 nanopores within the topograph (Figure 1a) spaced at 500 nm distances, corresponding to the diameter of the surface mask. A hexagonal arrangement of seven nanopores is shown in Figure 1b. The shapes are not perfectly round and symmetric at the nanoscale; rather the roughness and slight imperfections of the underlying substrate influence the shape. The nanostructures with regular circular geometries occur at sites of flat terraces without scars or terrace edges. A magnified view of an individual nanopore is shown in Figure 1c, and an example cursor profile across the nanopore is shown in Figure 1d. The images in Figure 1 are representative of multiple areas of the sample. The areas of nanopores provide an opportunity to obtain multiple measurements of the local film thickness to obtain a representative value. The average depth measured 2.6 ± 0.2 nm (n = 40) for the polyphenylene film prepared with the selected reaction conditions. The average value was derived by obtaining a representative cursor measurement across the central area of individual nanopores acquired along the horizontal scan direction of the image, n refers to the number of nanopores measured.

Effect of Increased NBDT Concentration for Film Thickness. One would predict that increasing either the concentration or the irradiation time would correspondingly produce a thicker film of polynitrophenylene. To test this hypothesis, further experiments with particle lithography were conducted to evaluate the parameters of concentration and light exposure while keeping the other parameters unchanged. The effects of increasing the concentration by 100-fold (0.1 M NBDT) after a 5 min irradiation time are shown in Figure 2. The morphology of the film appears relatively smooth and dense. The domain boundaries and scars of the underlying substrate are not evident for the sample in Figure 2, which was prepared using template-stripped gold. The process of gluing glass to the ultraflat gold film and stripping it from the mica substrate provided a distinctly flat and uniform surface morphology. For thicker surface films, the substrate features are likely to be indistinguishable. There are 91 nanopores within the 6 × 6 μm^2 topography image shown in Figure 2a. The uncovered sites became more prominent, with clearly resolved edges. A comparison of surface chemistry is mapped in lateral force images rather than changes in height. Corresponding differences in frictional forces between the AFM probe and surface groups are mapped in the lateral force image (Figure 2b). The bright areas are the uncovered areas of the gold substrate measuring ∼18% coverage of the surface. The areas of the polynitrophenylene film are darker and homogeneous in color, suggesting a fairly uniform chemical composition throughout the sample. A close-up view of three nanopores is

dx.doi.org/10.1021/ja505521k | J. Am. Chem. Soc. 2014, 136, 14438−14444

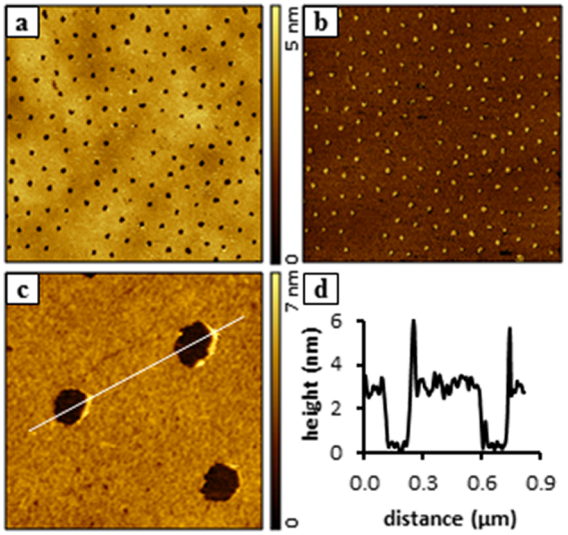

Figure 2. Nanopores within a polynitrophenylene film formed with 0.1 M NBDT after 5 min of irradiation. (a) Topography and (b) corresponding lateral force images (6 × 6 μm^2); (c) zoom-in view of nanopores (750 × 750 nm^2); (d) cursor profile for the line in panel c.

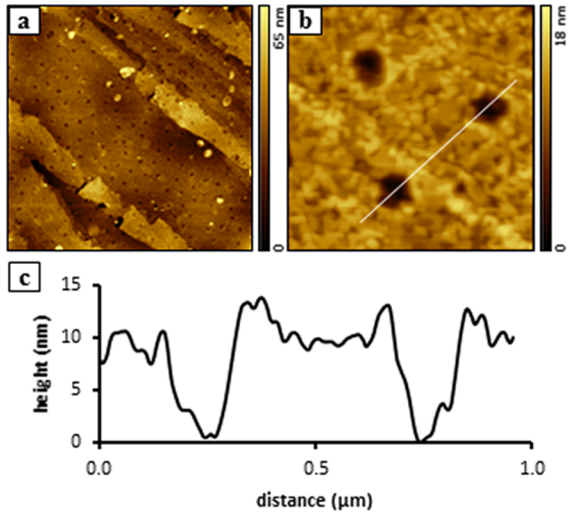

Figure 3. Photografted film of polynitrophenylene punctuated with nanopores prepared with 15 min irradiation in 0.1 M NBDT. (a) Topography image (5 × 5 μm^2); (b) zoom-in topograph (750 × 750 nm^2); (c) cursor profile across two nanopores in panel b.

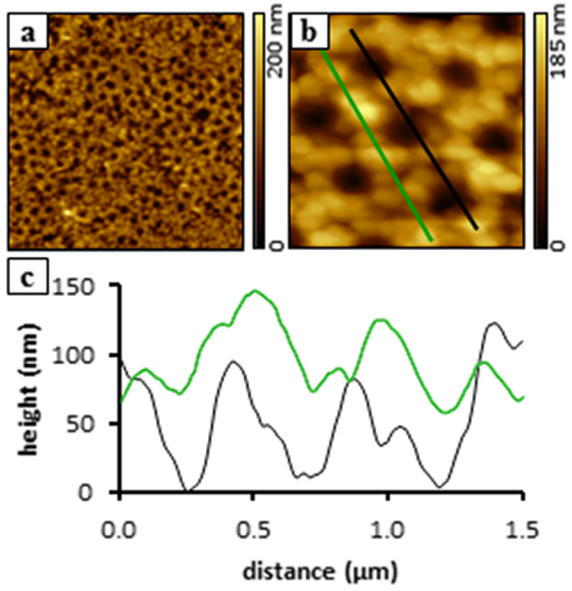

Figure 4. Polynitrophenylene film prepared with an irradiation time of 30 min in 0.1 M NBDT. (a) Topography image (6.5 × 6.5 μm^2) acquired in air; (b) zoom-in view (1.25 × 1.25 μm^2); (c) cursor profiles for the lines in panel b.

shown in Figure 2c, revealing a regular and smooth morphology for the photografted film. The diameter of the nanopores measured 77 ± 14 nm (n = 38), which closely matches the experiment in Figure 1. The depths of the nanopores measured 3 ± 0.2 nm (n = 49), shown with an example cursor profile in Figure 2d.

In previous reports with electrochemically grafted films, the compactness or density was greater with increasing diazonium salt concentration.[43,53] With electrochemical grafting, high concentrations of diazonium salts can produce multilayer films after longer reduction times.[54] Comparing the two experiments shown in Figures 1 and 2, changing the parameters of immersion time, as well as increasing the diazonium and catalyst concentrations, did not greatly increase the overall film thickness; however, the film in Figure 2 appears to be more dense and compact.

Effect of Increased Irradiation Time for Film Thickness. The parameter of increasing the irradiation time was tested using 0.1 M NBDT for the experiment shown in Figure 3. After 15 min of irradiation, AFM images of the polynitrophenylene film revealed a less regular topography and thicker layer (Figure 3a). Thicker areas formed an arrangement of strips across areas of the sample with areas of flatter domains in between the ridges. Zooming-in for a closer view, the areas of polymer have a rougher, clustered morphology (Figure 3b). The nanopores can still be distinguished as dark spots throughout areas of the sample within a dense film. A representative line profile across two of the nanopores is shown in Figure 3c, with the thickness of the film measured to be 13 ± 2 nm (n = 49).

When the reaction time was further increased to 30 min while maintaining an initial concentration of 0.1 M NBDT, the film morphology and thickness changed substantially (Figure 4). The morphology of the thicker film of polynitrophenylene is no longer smooth and continuous. A rougher, irregular arrangement of surface structures surrounding nanopores is apparent in Figure 4a. Within a magnified view (Figure 4b), a honeycomb arrangement of seven nanopores is disclosed with polymer clusters surrounding the bowl-shaped nanopores. The thickness of the film measured 89 ± 22 nm (n = 46). An example cursor profile is shown in Figure 4c; however, the irregularly shaped edges of nanopores cannot be fully represented with a single line scan. Therefore, an additional line trace is presented for an area without nanopores. Using the bottom of the nanopores as a baseline, the range of heights measured from 57 to 163 nm (n = 46).

By changing the duration of irradiation for time intervals on the order of a few minutes, considerable increases in film thickness were detected. A comparison of the film thickness for selected irradiation times is shown in Figure 5, referencing the bottom of nanopores as a baseline. The error bars were determined from the standard deviation of the measurements. The chart effectively demonstrates the sensitivity to changes in the duration of light exposure for the photografting reaction

dx.doi.org/10.1021/ja505521k | J. Am. Chem. Soc. 2014, 136, 14438−14444

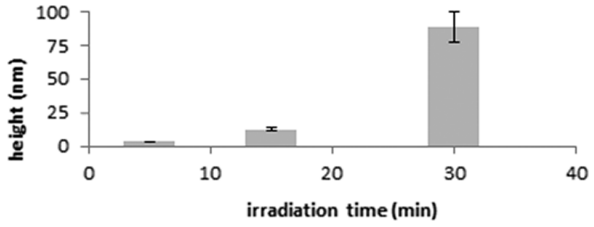

Figure 5. Thickness of the polynitrophenylene films measured at different irradiation times for samples prepared with 0.1 M NBDT.

with diazonium salts. As irradiation time was increased, the thickness of the film increased within an overall time frame of 30 min. For the parameter of the concentration of NBDT, the differences in the thickness of the film were not as large. The film formed with a starting concentration of 0.001 M NBDT measured 2.6 ± 0.2 nm in thickness (30 min irradiation), whereas the film prepared with 0.1 M NBDT (5 min irradiation) measured 3.2 ± 0.2 nm. The difference in thickness of 0.6 nm corresponds approximately to the addition of a single phenylene group.

Two control experiments were run to evaluate the progress of the reaction without catalyst (Supporting Information, Figure S4) and without illumination (Supporting Information, Figure S5). The spontaneous grafting of the diazonium salt was evaluated using 0.1 M NBDT for 30 min reaction time. The control sample prepared without catalyst (Figure S4) did evidence spontaneous grafting of polyphenylene at areas near the meniscus sites of the mesosphere masks, with thicknesses ranging from 1 to 3 nm. The control sample prepared without visible light illumination (Figure S5) showed evidence for the spontaneous grafting of polyphenylene at areas throughout the sample, measuring 7 ± 2 nm in thickness.

Grafting of diazonium salts using electrochemical reduction is primarily a diffusion-controlled process.[4] Reduction of the diazonium cation by the substrate produces an aryl radical that couples to the surface for growth of an organic film. Multilayers are generated as the reaction proceeds with phenyl radicals attaching to the surface-bound molecules, forming covalent carbon−carbon bonds.[54] Once the multilayer film has reached a thickness at which electron transfer through the surface film is no longer possible, the growth will terminate.[18] With electrochemical reduction, additional surface layers can restrict reduction of further molecules at the surface. Photocatalysis, on the other hand, continuously produces radicals to graft either to the surface or to grafted molecular layers to effect continuous growth under conditions of irradiation with visible light. The growth can effectively be switched off by removing the light source. In our experiments, an increase in film thickness was observed when the duration of light exposure was increased, while keeping all other parameters constant. Surface layers up to 100 nm in thickness are accessible with catalytic photografting because the growth of multilayers is not limited by a reduction in conductivity as it is with electrografting.[55]

Backfilling Exposed Sites of Au(111) with Mercaptoundecanoic Acid. The exposed surfaces sites of the substrate located within the nanopores can be filled with selected molecules to generate nanostructures with designed chemical groups. An ω-functionalized *n*-alkanethiol which contains a carboxylic acid headgroup was chosen for backfilling. MUA in ethanol (0.6 mM) was added to the sample shown in Figure 2 (0.1 M NBDT, 5 min irradiation). A close-up view of the sample is presented in Figure 6a, revealing the shapes and

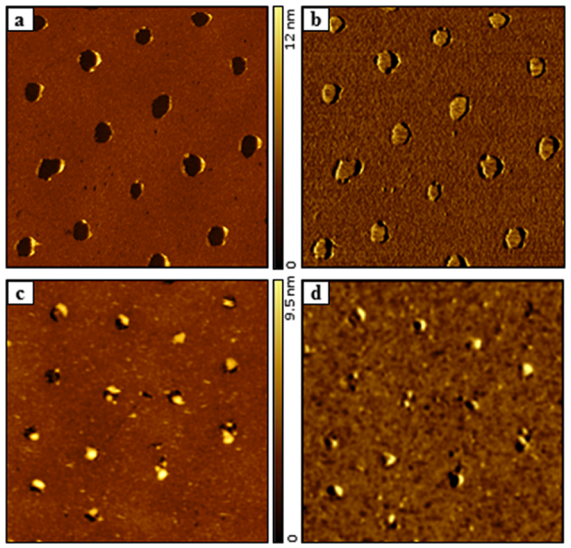

Figure 6. After backfilling with an *n*-alkanethiol, nanostructures formed within exposed sites of the nanopores. (a) Topography image of nanopores within a matrix film of polynitrophenylene (2 × 2 μm^2); (b) simultaneously acquired lateral force image; (c) topography after backfilling with MUA (2 × 2 μm^2); (d) corresponding lateral force image.

arrangement of 16 nanopores within the film of polynitrophenylene. The shapes of the nanoscopic surface sites of exposed Au(111) can be clearly distinguished in the lateral force frame (Figure 6b). After 24 h of immersion in MUA, clusters of molecules attached within the exposed areas of the sample (Figure 6c). A few of the sites have multiple islands within the nanopores which can be resolved in the lateral force image (Figure 6d). After backfilling, the area that was selected for imaging has shifted; the frames in Figure 6c,d contain 14 nanostructures within an area of 2 × 2 μm^2, which would scale to a surface density of ~10^8 nanopores/cm^2.

A side-by-side comparison of the stability of the diazonium-derived film versus thiol-bound MUA was accomplished with the backfilled sample of Figure 6. An experiment was designed to use the force of an AFM probe to shave regions of the sample. Thiolated molecules can be displaced from the surface using a process known as nanoshaving.[56] Local areas of surface films can be shaved away to expose the substrate by increasing the force on the probe. Steps of the nanoshaving process are shown with AFM topography frames in Figure 7. An example image of a single nanostructure of MUA is shown in Figure 7a. Before backfilling with MUA, the depth of the nanopore measured 3.0 ± 0.2 nm (n = 49). Under low force, images can be acquired without disturbing the shapes of the nanostructures. After immersion in MUA solution for 24 h, a nanostructure measuring 8.7 nm was formed (Figure 7b). The height corresponds to the thickness of a multilayer of MUA formed by interactions between acid headgroups. Nanostructures of multiple layers of MUA were previously observed to form under certain conditions as reported by Kelley et al.[57] The area containing the nanostructure and surrounding matrix film (500 × 500 nm^2) was scanned at higher force (swept 20 times) to shave away the surface film. The force was sufficient to remove thiol molecules; however, the photografted film of polynitrophenylene persisted, as shown in the representative image in Figure 7c. Some of the displaced molecules from the nanostructure remained at the edge of the

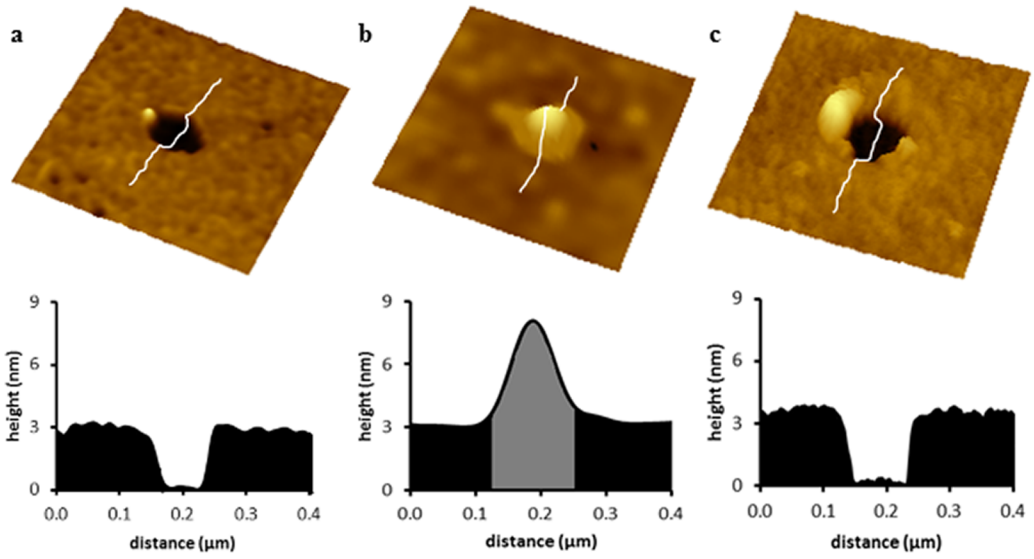

Figure 7. Steps for backfilling and shaving the nanopores filled with MUA. Topography images (500 × 500 nm^2) of (a) a single nanopore within the polynitrophenylene matrix film; (b) nanostructure of MUA formed within a nanopore; (c) the same area of the MUA nanostructure after nanoshaving. The local areas of nanopore are not the same for the *ex situ* experiments.

pattern. The thickness of the polynitrophenylene film after nanoshaving (Figure 7c) matches the thickness measured before nanoshaving (Figure 7a).

Under certain experimental conditions, aryl films formed from the reduction of diazonium salts were bonded to gold surfaces more strongly compared to equivalent thiol-bound films, as reported by Shewchuk et al.[2] For the experiment in Figure 7, after nanoshaving, the polynitrophenylene film persisted on the gold surface while the MUA nanostructure was removed by the sweeping action of the AFM tip. The photografted film provided spatial selectivity as a matrix film. No evidence of self-exchange or adsorption of MUA on areas between the nanostructures was visible throughout the course of a 24 h experiment.

CONCLUSIONS

Nanopores within polynitrophenylene films on Au(111) surfaces were prepared using visible light photocatalysis combined with particle lithography. To accomplish nanolithography, substrates were masked with a film of silica mesospheres to protect local areas of the surface from polymer deposition. Solutions of *p*-nitrobenzenediazonium tetrafluoroborate and the photoredox catalyst $Ru(bpy)_3(PF_6)_2$ were irradiated to produce *p*-nitrophenyl radicals that graft onto masked substrates of Au(111). Within only a few minutes of irradiation, samples were generated with exquisite arrangements of periodic nanopores within densely packed films of polynitrophenylene. The depth of nanopores was used to evaluate film thickness, which was found to depend sensitively on the parameter of irradiation time. The nanopores were filled with a second molecule with thiol−gold chemisorption (MUA), generating a surface with designed interfacial chemistry.

ASSOCIATED CONTENT

Supporting Information

Figures S1 and S2, ^{1}H and ^{13}C NMR spectra for NBDT, respectively; Figure S3, photo of the apparatus used for immersion of gold substrates; and Figures S4 and S5, control experiments of the reaction conducted without catalyst and without illumination, respectively. This material is available free of charge via the Internet at http://pubs.acs.org.

AUTHOR INFORMATION

Corresponding Author

jragains@lsu.edu

Notes

The authors declare no competing financial interest.

ACKNOWLEDGMENTS

The authors gratefully acknowledge support from the National Science Foundation Career/PECASE award (CHE-0847291), the American Chemical Society Petroleum Research Fund New Directions Program (52305-ND), the Camille Dreyfus Teacher-Scholar Program, and the Louisiana Board of Regents RCS support fund (LEQSF(2013-16)-RD-A-03). We thank Ms. Chelsea Eaton for assistance with the synthesis of NBDT.

REFERENCES

(1) Liu, G.; Böcking, T.; Gooding, J. J. *J. Electroanal. Chem.* **2007**, *600*, 335−344.
(2) Shewchuk, D. M.; McDermott, M. T. *Langmuir* **2009**, *25*, 4556−4563.
(3) Haccoun, J.; Vautrin-Ul, C.; Chaussé, A.; Adenier, A. *Prog. Org. Coat.* **2008**, *63*, 18−24.
(4) Bousquet, A.; Ceccato, M.; Hinge, M.; Pedersen, S. U.; Daasbjerg, K. *Langmuir* **2012**, *28*, 1267−1275.
(5) Kullapere, M.; Marandi, M.; Sammelselg, V.; Menezes, H. A.; Maia, G.; Tammeveski, K. *Electrochem. Commun.* **2009**, *11*, 405−408.
(6) Lyskawa, J.; Bélanger, D. *Chem. Mater.* **2006**, *18*, 4755−4763.
(7) Matrab, T.; Chehimi, M. M.; Perruchot, C.; Adenier, A.; Guillez, A.; Save, M.; Charleux, B.; Cabet-Deliry, E.; Pinson, J. *Langmuir* **2005**, *21*, 4686−4694.
(8) Allongue, P.; Henry de Villeneuve, C.; Cherouvrier, G.; Cortés, R.; Bernard, M.-C. *J. Electroanal. Chem.* **2003**, *550*−*551*, 161−174.
(9) Ghorbal, A.; Grisotto, F.; Laudé, M.; Charlier, J.; Palacin, S. *J. Colloid Interface Sci.* **2008**, *328*, 308−313.
(10) Brooksby, P. A.; Downard, A. J. *Langmuir* **2005**, *21*, 1672−1675.
(11) Picot, M.; Nicolas, I.; Poriel, C.; Rault-Berthelot, J.; Barrière, F. *Electrochem. Commun.* **2012**, *20*, 167−170.

(12) Boland, S.; Barrière, F.; Leech, D. *Langmuir* **2008**, *24*, 6351−6358.
(13) Fontaine, O.; Ghilane, J.; Martin, P.; Lacroix, J.-C.; Randriamahazaka, H. *Langmuir* **2010**, *26*, 18542−18549.
(14) Liu, G.; Wang, S.; Liu, J.; Song, D. *Anal. Chem.* **2012**, *84*, 3921−3928.
(15) Nielsen, L. T.; Vase, K. H.; Dong, M.; Besenbacher, F.; Pedersen, S. U.; Daasbjerg, K. *J. Am. Chem. Soc.* **2007**, *129*, 1888−1889.
(16) Lee, L.; Brooksby, P. A.; Leroux, Y. R.; Hapiot, P.; Downard, A. J. *Langmuir* **2013**, *29*, 3133−3139.
(17) Dunér, G.; Iruthayaraj, J.; Daasbjerg, K.; Pedersen, S. U.; Thormann, E.; Dėdinaitė, A. *J. Colloid Interface Sci.* **2012**, *385*, 225−234.
(18) Lehr, J.; Williamson, B. E.; Downard, A. J. *J. Phys. Chem. C* **2011**, *115*, 6629−6634.
(19) Uetsuka, H.; Shin, D.; Tokuda, N.; Saeki, K.; Nebel, C. E. *Langmuir* **2007**, *23*, 3466−3472.
(20) Ghilane, J.; Delamar, M.; Guilloux-Viry, M.; Lagrost, C.; Mangeney, C.; Hapiot, P. *Langmuir* **2005**, *21*, 6422−6429.
(21) Maldonado, S.; Smith, T. J.; Williams, R. D.; Morin, S.; Barton, E.; Stevenson, K. J. *Langmuir* **2006**, *22*, 2884−2891.
(22) Haque, A.-M. J.; Kim, K. *Chem. Commun.* **2011**, *47*, 6855−6857.
(23) Kariuki, J. K.; McDermott, M. T. *Langmuir* **1999**, *15*, 6534−6540.
(24) Bradbury, C. R.; Kuster, L.; Fermín, D. J. *J. Electroanal. Chem.* **2010**, *646*, 114−123.
(25) Bernard, M. C.; Chaussé, A.; Cabet-Deliry, E.; Chehimi, M. M.; Pinson, J.; Podvorica, F.; Vautrin-Ul, C. *Chem. Mater.* **2003**, *15*, 3450−3462.
(26) Santos, L.; Ghilane, J.; Lacroix, J. C. *J. Am. Chem. Soc.* **2012**, *134*, 5476−5479.
(27) Kullapere, M.; Marandi, M.; Matisen, L.; Mirkhalaf, F.; Carvalho, A. E.; Maia, G.; Sammelselg, V.; Tammeveski, K. *J. Solid State Electrochem.* **2012**, *16*, 569−578.
(28) Yu, S. S. C.; Downard, A. J. *J. Surf. Sci. Nanotechnol.* **2005**, *3*, 294−298.
(29) Chen, H.; Wang, Y.; Qu, J.; Dong, S. *J. Raman Spectrosc.* **2007**, *38*, 1444−1448.
(30) Mahouche-Chergui, S.; Gam-Derouich, S.; Mangeney, C.; Chehimi, M. M. *Chem. Soc. Rev.* **2011**, *40*, 4143−4166.
(31) Zhao, W.; Tong, B.; Pan, Y.; Shen, J.; Zhi, J.; Shi, J.; Dong, Y. *Langmuir* **2009**, *25*, 11796−11801.
(32) Evrard, D.; Lambert, F.; Policar, C.; Balland, V.; Limoges, B. *Chem.—Eur. J.* **2008**, *14*, 9286−9291.
(33) Cernat, A.; Griveau, S.; Martin, P.; Lacroix, J. C.; Farcau, C.; Sandulescu, R.; Bedioui, F. *Electrochem. Commun.* **2012**, *23*, 141−144.
(34) Bouriga, M.; Chehimi, M. M.; Combellas, C.; Decorse, P.; Kanoufi, F.; Deronzier, A.; Pinson, J. *Chem. Mater.* **2013**, *25*, 90−97.
(35) Schroll, P.; Fehl, C.; Dankesreiter, S.; König, B. *Org. Biomol. Chem.* **2013**, *11*, 6510−6514.
(36) Hari, D. P.; König, B. *Angew. Chem., Int. Ed.* **2013**, *52*, 4734−4743.
(37) Garcia, A.; Hanifi, N.; Jousselme, B.; Jegou, P.; Palacin, S.; Viel, P.; Berthelot, T. *Adv. Funct. Mater.* **2013**, *23*, 3668−3674.
(38) Park, E. J.; Wagenaar, T.; Zhang, S.; Link, A. J.; Prud'homme, R. K.; Koberstein, J. T.; Turro, N. J. *Langmuir* **2012**, *28*, 10934−10941.
(39) Busson, M.; Berisha, A.; Combellas, C.; Kanoufi, F.; Pinson, J. *Chem. Commun.* **2011**, *47*, 12631−12633.
(40) Azevedo, J.; Fillaud, L.; Bourdillon, C.; Noël, J.-M.; Kanoufi, F.; Jousselme, B.; Derycke, V.; Campidelli, S.; Cornut, R. *J. Am. Chem. Soc.* **2014**, *136*, 4833−4836.
(41) Garrett, D. J.; Lehr, J.; Miskelly, G. M.; Downard, A. J. *J. Am. Chem. Soc.* **2007**, *129*, 15456−15457.
(42) Lehr, J.; Garrett, D. J.; Paulik, M. G.; Flavel, B. S.; Brooksby, P. A.; Williamson, B. E.; Downard, A. J. *Anal. Chem.* **2010**, *82*, 7027−7034.
(43) Anariba, F.; DuVall, S. H.; McCreery, R. L. *Anal. Chem.* **2003**, *75*, 3837−3844.
(44) Charlier, J.; Palacin, S.; Leroy, J.; Del Frari, D.; Zagonel, L.; Barrett, N.; Renault, O.; Bailly, A.; Mariolle, D. *J. Mater. Chem.* **2008**, *18*, 3136−3142.
(45) Corgier, B. P.; Bélanger, D. *Langmuir* **2010**, *26*, 5991−5997.
(46) Santos, L.; Ghilane, J.; Lacroix, J.-C. *Electrochem. Commun.* **2012**, *18*, 20−23.
(47) Saner, C. K.; Lusker, K. L.; LeJeune, Z. M.; Serem, W. K.; Garno, J. C. *Beilstein J. Nanotechnol.* **2012**, *3*, 114−122.
(48) Pangborn, A. B.; Giardello, M. A.; Grubbs, R. H.; Rosen, R. K.; Timmers, F. J. *Organometallics* **1996**, *15*, 1518−1520.
(49) Wagner, P.; Zaugg, F.; Kernen, P.; Hegner, M.; Semenza, G. *J. Vac. Sci. Technol. B* **1996**, *14*, 1466−1471.
(50) Vogel, A. I. *Practical Organic Chemistry*, 5th ed.; John Wiley and Sons, Inc.: New York, 1989.
(51) Nečas, D.; Klapetek, P. *Central Eur. J. Phys.* **2012**, *10*, 181−188.
(52) Poirier, G. E. *Langmuir* **1997**, *13*, 2019−2026.
(53) Saby, C.; Ortiz, B.; Champagne, G. Y.; Bélanger, D. *Langmuir* **1997**, *13*, 6805−6813.
(54) Kariuki, J. K.; McDermott, M. T. *Langmuir* **2001**, *17*, 5947−5951.
(55) Ceccato, M.; Bousquet, A.; Hinge, M.; Pedersen, S. U.; Daasbjerg, K. *Chem. Mater.* **2011**, *23*, 1551−1557.
(56) Liu, G. Y.; Xu, S.; Qian, Y. L. *Acc. Chem. Res.* **2000**, *33*, 457−466.
(57) Kelley, A. T.; Ngunjiri, J. N.; Serem, W. K.; Lawrence, S. O.; Yu, J. J.; Crowe, W. E.; Garno, J. C. *Langmuir* **2010**, *26*, 3040−3049.